ACS OMEGA

http://pubs.acs.org/journal/acsodf

Article

Three-Dimensional Graphene–TiO_2–SnO_2 Ternary Nanocomposites for High-Performance Asymmetric Supercapacitors

Golnoush Zamiri,* A.S. Md. Abdul Haseeb,* Priyanka Jagadish, Mohammad Khalid, Ing Kong, and Syam G. Krishnan*

Cite This: *ACS Omega* 2022, 7, 43981–43991

Read Online

ACCESS | Metrics & More | Article Recommendations | Supporting Information

ABSTRACT: Ternary nanocomposites synergistically combine the material characteristics of three materials, altering the desired charge storage properties such as electrical conductivity, redox states, and surface area. Therefore, to improve the energy synergistic of SnO_2, TiO_2, and three-dimensional graphene, herein, we report a facile hydrothermal technique to synthesize a ternary nanocomposite of three-dimensional graphene–tin oxide–titanium dioxide (3DG–SnO_2–TiO_2). The synthesized ternary nanocomposite was characterized using material characterization techniques such as XRD, Raman spectroscopy, FTIR spectroscopy, FESEM, and EDXS. The surface area and porosity of the material were studied using Brunauer–Emmett–Teller (BET) studies. XRD studies showed the crystalline nature of the characteristic peaks of the individual materials, and FESEM studies revealed the deposition of SnO_2–TiO_2 on 3DG. The BET results show that incorporating 3DG into the SnO_2–TiO_2 binary nanocomposite increased its surface area compared to the binary composite. A three-electrode system compared the electrochemical performances of both the binary and ternary composites as a battery-type supercapacitor electrode in different molar KOH (1, 3, and 6 M) electrolytes. It was determined that the ternary nanocomposite electrode in 6 M KOH delivered a maximum specific capacitance of 232.7 C g^{-1} at 1 A g^{-1}. An asymmetric supercapacitor (ASC) was fabricated based on 3DG–SnO_2–TiO_2 as a positive electrode and commercial activated carbon as a negative electrode (3DG–SnO_2–TiO_2//AC). The ASC delivered a maximum energy density of 28.6 Wh kg^{-1} at a power density of 367.7 W kg^{-1}. Furthermore, the device delivered a superior cycling stability of ∼97% after 5000 cycles, showing its prospects as a commercial ASC electrode.

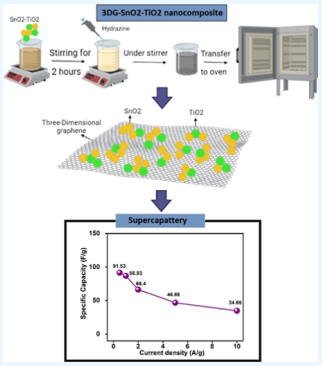

INTRODUCTION

Transformation of technologies from wired to wireless communication devices and fossil fuel-sourced transportation to electric vehicles require efficient energy storage devices.[1] For a longer duration energy release process (higher energy density), lithium-ion batteries (LIB) are currently preferred. Redox reactions involving electrode–electrolyte surfaces due to the intercalation–deintercalation process of Li ions store charges in LIBs as chemical energy. Although LIBs are accompanied by higher energy densities, their lower power density hinders their high power applications.[2] Supercapacitors, another energy storage subclass, have gained prominence due to their increased power density, rapid charging/discharging, and long cyclic efficiency, along with their increased environmental friendliness and relatively low cost.[3] However, the low energy density limited the use of supercapacitors in many applications.[4] From this perspective, it is critical to increase energy density by developing a hybrid energy storage device, known as an ssymmetric supercapacitor (ASC), which combines the characteristics of both supercapacitors and batteries.[5] A typical ASC consists of battery-grade materials (redox-active materials enabling faradaic reaction processes) as a positive electrode (high energy density) and carbonaceous materials such as activated carbon (high power density) as a negative electrode.[6]

Several redox-active metal oxides such as NiO, RuO_2, MnO_2, TiO_2, Co_3O_4, SnO_2, and so forth were utilized for high-performance energy storage devices.[7] Among these metal oxides, TiO_2 and SnO_2 are excellent candidates for electrode materials due to their low cost and environmental friendliness. Furthermore, these possess negligible volume expansion during the discharge–charge process, resulting in long cycle life and durability.[8] However, pure SnO_2 and TiO_2 nanostructures have low electronic conductivity, poor electrochemical stability, low rate capability, and relatively low theoretical capacity, limiting their industrial application.[9] Synergistically combining the properties of two or more materials is proven to be one of the effective ways to overcome the obstacles of pure SnO_2 and TiO_2. A recent research report on the electrospun binary composites of SnO_2–TiO_2 3D nanoflowers showed higher

Received: August 20, 2022
Accepted: November 14, 2022
Published: November 23, 2022

specific capacitance (500 F g^{-1}) than nanofibers (350 F g^{-1}) at 1 A g^{-1}, showing the superiority of the 3D structure.[10] However, the rate capability of the SnO_2−TiO_2 electrode was lower, achieving a lower capacitance at higher current densities.[11] The performance of supercapacitors can be enhanced by incorporating the high surface area of carbon-based materials into metal oxide nanostructures.[12] Nowadays, the fabrication of three-dimensional graphene (3DG) with high surface area, low density, and high electrical conductivity is increasingly receiving research attention.[13] Intercalation of metal oxides with graphene-based materials including 3DG provides more electrochemically active sites for rapid redox processes and conducting networks, as well as the benefit of reducing the risk of large volume changes during a charge−discharge mechanism.[14] For example, 3DG-NiO nanocomposite electrodes with a high specific capacitance of 1328 F g^{-1} at a current density of 1 A g^{-1} have been fabricated by Bao et al[15] The device shows cycling stability with 87% retention of the capacitance after 2000 cycles of galvanostatic charge−discharge. Furthermore, the importance of 3DG was further iterated by Jiang and his group by synthesizing the 3DG−TiO_2 nanocomposite.[16] The 3DG−TiO_2 composite electrode obtained a specific capacitance of 235.6 F g^{-1} at 0.5 A g^{-1} in 2 M KOH and delivered a rate capability of 87% after 2000 cycles of charge−discharge. Therefore, in general, nanocomposites based on 3DG achieved appreciable specific capacitance, and the rate capability of these devices was improved by adding 3DG to the composites. However, most of the reported composites exhibited poor cyclic stability (less than 80%).

In this research, a novel attempt to improve the charge storage process of SnO_2−TiO_2 was performed using 3DG. A ternary nanocomposite of SnO_2−TiO_2 with 3DG (3DG−SnO_2−TiO_2) was prepared by the hydrothermal method for the first time, and the electrochemical performance of the 3DG−SnO_2−TiO_2 ternary nanocomposite using 6 M KOH as an electrolyte was investigated. An increase in surface area of the SnO_2−TiO_2 composite was observed with the addition of 3DG into it. This addition shall increase the active surface of the binary composite, providing more active sites for the solvated electrolytes to access. Hence, in the three-electrode system, the ternary nanocomposite of 3DG−SnO_2−TiO_2 exhibited a higher specific capacity compared to the binary nanocomposite of SnO_2−TiO_2. Finally, an ASC was fabricated based on the 3DG−SnO_2−TiO_2 ternary nanocomposite for the first time, which showed good electrochemical performance and superior cycling stability.

2. EXPERIMENTAL SECTION

2.1. Materials. Graphite flakes were purchased from Asbury Inc. (USA). All the experimental chemicals such as aniline, hydrogen peroxide (H_2O_2), ammonium persulfate (APS), poly (vinylidene fluoride) (PVDF), activated carbon (AC), hydrazine, nickel foam, potassium permanganate ($KMnO_4$), sulfuric acid (H_2SO_4), hydrochloric acid (HCl), potassium hydroxide pellets (KOH), phosphoric acid (H_3PO_4), *N*-methyl-2-pyrrolidone (NMP), tin chloride hydrate, and titanium isopropoxide were supplied by Sigma-Aldrich, USA.

2.2. Preparation of the SnO_2−TiO_2 Nanocomposite. To prepare the binary nanocomposite of SnO_2−TiO_2, 1:1 M mixture of tin chloride hydrate ($SnCl_4{\cdot}5H_2O$) and titanium isopropoxide ($C_{12}H_{28}O_4Ti$) was added to the mixture of ethanol and dimethylformamide (DMF). Then, the mixture was stirred vigorously for 24 h at room temperature to form a homogeneous solution. After that, the solution was transferred to a 50 mL Teflon-lined autoclave and heated at 75 °C for 24 h. The autoclave was naturally cooled to room temperature, and the prepared SnO_2−TiO_2 nanocomposite was washed with distilled water and ethanol.

2.3. Preparation of the 3DG−SnO_2−TiO_2 Ternary Nanocomposite. Initially, graphene oxide (GO) was synthesized from graphite flakes by using a modified Hummers method.[17] For the 3DG−SnO_2−TiO_2 nanocomposite preparation, 50 mL of distilled water and the prepared GO (1 mg/mL) were mixed under stirring for 2 h, and 50 mg of the SnO_2−TiO_2 nanocomposite was added to the mixture. After that, 10 μL of hydrazine was slowly dropped into the solution and continued stirring for 20 min. Then, it was transferred to a 50 mL Teflon-lined autoclave and heated at 75 °C for 24 h. The prepared ternary nanocomposite of 3DG−SnO_2−TiO_2 was filtered and washed several times with distilled water and ethanol. After the purification process, the final product was freeze-dried for 48 h.[18,19]

2.4. Material Characterization. An X-ray diffractometer (Philips X'pert) with Cu−K X-ray radiation (=1.5418 A°) in the range of 10−70 degrees of 2-theta was used to examine the crystalline structures of the materials. Using a Fourier transform infrared (FT-IR) spectrometer (model: Bruker IFS 66/S), the presence of various functional groups in the produced samples was investigated. An FESEM instrument (JEOL JSM-7600F) equipped with an Oxford energy-dispersive X-ray spectroscopy system was used to characterize the morphology and elemental mapping (EDS). A surface area analyzer (Brunauer−Emmett−Teller (BET)) was used to determine the specific surface area and pore size and volume distribution of 3DG, the SnO_2−TiO_2 binary nanocomposite, and the 3DG−SnO_2−TiO_2 ternary nanocomposite.

2.5. Electrochemical Measurements. The working electrodes were made by combining the as-prepared materials (SnO_2−TiO_2 and 3DG−SnO_2−TiO_2), carbon black, and PVDF in a 75:15:10 weight ratio, with NMP as the solvent. This mixture was stirred for 12 h before being pasted onto an area of 1 cm^2 of precleaned nickel foam and dried at 80 °C for 12 h. The mass loading of SnO_2−TiO_2 and 3DG−SnO_2−TiO_2 was 4.8 and 2.7 mg, respectively. At room temperature, the electrochemical performance of the fabricated electrode was tested on an electrochemical workstation (Metrohm Autolab PGSTAT 302N) equipped with a three-electrode cell system containing a working electrode (binary and ternary composite), Ag/AgCl electrode as a reference, and a platinum wire as a counter electrode. The electrolyte used for the analysis was 1, 3, and 6 M KOH. The CV curves were recorded at different scan rates (3, 5, 10, 20, 30, 40, and 50 mV/s) within a specific potential window for both the three-electrode system and the ASC device. The GCD analysis was performed at different current densities ranging from 0.5 to 10 A g^{-1}. The EIS measurement was performed at frequencies ranging between 0.01 and 100 kHz with an ac perturbation of 10 mV.

3. RESULTS AND DISCUSSION

3.1. Structural and Morphological Characteristics of Materials. The FTIR spectra of SnO_2−TiO_2 and 3DG−SnO_2−TiO_2 are shown in Figure 1. The broad peak from 3000 to 3600 cm^{-1} in the FTIR spectra of both SnO_2−TiO_2 and 3DG−SnO_2−TiO_2 corresponds to the surface stretching

https://doi.org/10.1021/acsomega.2c05343
ACS Omega 2022, 7, 43981−43991

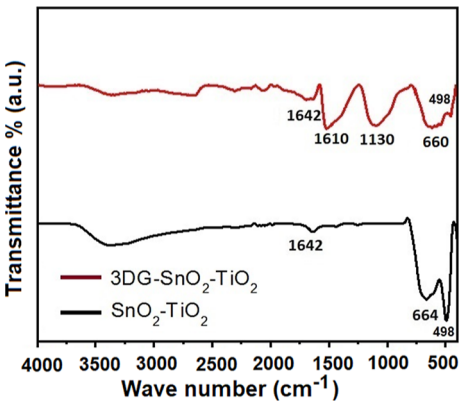

Figure 1. FTIR spectra of SnO_2−TiO_2 and 3DG−SnO_2−TiO_2 nanocomposites.

vibration by H_2O molecules or hydroxyl groups. The peak at 1642 cm^{-1} in both the as-prepared nanocomposites can be associated to the O−H vibration in absorbed water on the surface of the samples.[20] Compared to the SnO_2−TiO_2 nanocomposite, the FTIR spectrum of the 3DG−SnO_2−TiO_2 ternary nanocomposite indicates strong peaks at 1610 and 1130 cm^{-1}, which are attributed to the C=C and C−O stretching vibrations, respectively. This confirms the presence of 3DG in the 3DG−SnO_2−TiO_2 ternary nanocomposite.[21] However, the presence of C=C and C−O stretching vibrations leads to the incomplete reduction of the graphene sheet. Typically, the reduction of GO under chemical reduction conditions (reducing agents) causes reduced graphene oxide formation.[22] The absorption bands, appearing between 660−665 and 498 cm^{-1}, are attributed to the stretching vibrations of Sn−O−Sn and Ti−O−Ti, respectively.[23]

The XRD spectra of 3DG, SnO_2−TiO_2, and 3DG−SnO_2−TiO_2 nanocomposites are compiled in Figure 2. For 3DG, the

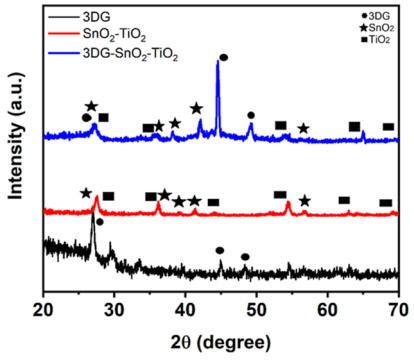

Figure 2. XRD patterns of pure 3DG, SnO_2−TiO_2, and 3DG−SnO_2−TiO_2 nanocomposites.

sharp peak at 26.9° and two weak peaks at 44.9 and 48.3° correspond to (002), (100), and (004) carbon reflections, respectively.[24] The peaks observed at around 28, 36, 42, 46, 52, 62.9, and 69.5° in the XRD patterns of SnO_2−TiO_2 and 3DG−SnO_2−TiO_2 nanocomposites are ascribed to the (110), (101), (111), (210), (211), (220), and (002) planes of the TiO_2 rutile phase. The four characteristic peaks at approximately 27, 37, 42, and 56° can be associated to the (110), (200), (211), and (220) planes of SnO_2, respectively.[25] The sharp and characteristic peak at around 45 and 49° in the 3DG−SnO_2−TiO_2 XRD pattern confirms the presence of 3DG in the ternary nanocomposite.[26] However, due to the overlapping (110) planes of TiO_2 and SnO_2, the characteristic peak of 3DG (002) is not observed in the XRD pattern of the ternary nanocomposite. Hence, the characteristic peaks of all the materials were well assimilated in the ternary composite, proving the formation of the 3DG−SnO_2−TiO_2 composite.

Figure 3 shows the Raman spectra of 3DG, SnO_2−TiO_2 binary, and 3DG−SnO_2−TiO_2 ternary nanocomposites. The

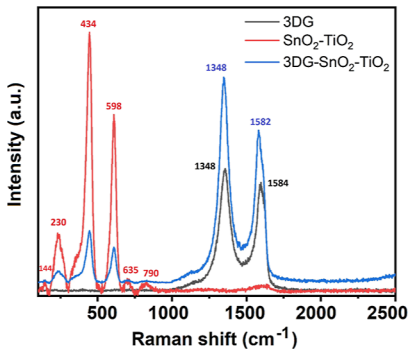

Figure 3. Raman spectra of 3DG, SnO_2−TiO_2, and 3DG−SnO_2−TiO_2 nanocomposites.

Raman spectra of 3DG displayed a D band at 1348 cm^{-1} that represents the sp^3 vibrations of C atoms of disordered graphene and a G peak at 1584 cm^{-1} which is related to the in-plane vibration of sp^2-bonded carbon atoms.[19] The *D* and *G* peak intensity ratio (I_D/I_G) indicates the quality of the products. The I_D/I_G intensity ratio increases from 1.13 of 3DG to 1.33 of the 3DG−SnO_2−TiO_2 ternary nanocomposite, which is related to a decrease in the average size of the sp^2 domains upon the reduction of the exfoliated GO, and this indicates the removal of oxygen groups.[27] The peaks appear at 144, 434, and 598 cm^{-1} in the Raman spectra of SnO_2−TiO_2 binary and 3DG−SnO_2−TiO_2 ternary nanocomposites corresponding to the system matrices of B_{1g}, E_g, and A_{1g} of the TiO_2 rutile phase, and another characteristic broad compound vibrational peak at 230 cm^{-1} aroused from the multiple phonon scattering processes.[28] In addition, the peaks at 630 and 774 cm^{-1} correspond to A_{1g} and B_{2g} modes of SnO_2, which are related to the symmetric and asymmetric stretching of Sn−O bonds, respectively.[29]

The surface morphologies of SnO_2−TiO_2 and 3DG−SnO_2−TiO_2 nanocomposites are shown in Figure 4. The FESEM images of SnO_2−TiO_2 showed irregular-shaped nanoparticles due to the agglomeration of tiny spherical shaped crystals. Figure 4c,d illustrates the FESEM images of 3DG−SnO_2−TiO_2 nanocomposites at low and high magnifications. The deposition of the SnO_2−TiO_2 nanocomposite on 3D graphene sheets was clearly visible (Figure 4d).

The EDX elemental mapping of the 3DG−SnO_2−TiO_2 ternary nanocomposite is shown in Figure 5a−f. The EDX analysis confirmed all the elemental components of the prepared 3DG−SnO_2−TiO_2 nanocomposite, as indicated in Figure 5a−e. The overall mapping in Figure 5a demonstrates the presence of C, O, Sn, and Ti, proving the elemental composition of the nanocomposite. Figure 5b shows the carbon distribution within the prepared nanocomposite. The presence of oxygen, Sn, and Ti elements in Figure 5c−e corresponds to the presence of the SnO_2−TiO_2 nanocomposite. From Figure 5d, it is observed that the Sn element

https://doi.org/10.1021/acsomega.2c05343
ACS Omega 2022, 7, 43981−43991

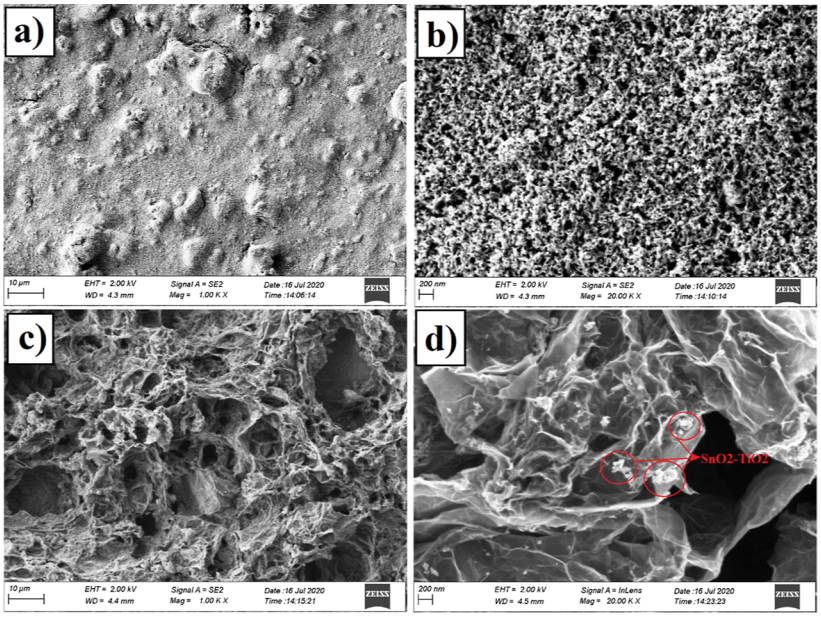

Figure 4. FESEM images of the SnO_2−TiO_2 nanocomposite at (a) low and (b) high magnifications and those of the 3DG−SnO_2−TiO_2 ternary nanocomposite at (c) low and (d) high magnifications.

homogeneously distributed in the nanocomposite. In comparison with the Sn element, the EDX elemental mapping of TiO_2 (Figure 5e) shows obvious particle agglomeration and volume expansion. The EDX image in Figure 5f shows the peaks of all elements such as C, O, Sn, and Ti in the ternary nanocomposite of 3DG−SnO_2−TiO_2, and the absence of any impurity peaks demonstrates the purity of the as-prepared nanocomposite.

The specific surface area of the prepared 3DG, SnO_2−TiO_2, and 3DG−SnO_2−TiO_2 nanocomposites was characterized using nitrogen gas adsorption and is illustrated in Figure 6. The specific surface area, calculated using the standard multipoint BET method, was 123.12, 63.50, and 72.21 m^2 g^{-1} for 3DG, SnO_2−TiO_2 nanocomposite, and 3DG−SnO_2−TiO_2 ternary nanocomposites, respectively. The surface area of the ternary nanocomposite is much lower than that of pure 3DG and slightly increased compared to the SnO_2−TiO_2 binary nanocomposite. This might be due to the amount of 3DG. Based on the literature,[30] by increasing the amount of graphene materials, the surface area of the nanocomposite will be further increased. The 3DG−SnO_2−TiO_2 ternary nanocomposite has a smaller pore size of 17.24 nm than the SnO_2−TiO_2 nanocomposite (21 nm). The existence of a mesoporous structure, with the pore size distribution center at 17.24 nm of the 3DG-SnO_2−TiO_2 ternary nanocomposite, can be observed in the inset of Figure 6. It is well established that the mesoporous structure with a higher surface area can provide excessive contacts between the electrode materials and the electrolyte, enhancing the expansion of ion transport pathways in the charge−discharge process, which is crucial to the rate capability of energy storage devices.[31]

3.2. Electrochemical Measurement. CV and GCD curves were recorded in a three-electrode system to evaluate the electrochemical performance of the 3DG−SnO_2−TiO_2 ternary nanocomposite and are shown in Figure 7. The energy storage properties of the prepared ternary nanocomposite using KOH as an electrolyte with various molarities (1, 3, and 6 M) were also investigated and indicated in Figures S1−S4. Based on the results, the specific capacity of the ternary nanocomposite in the various electrolytes decreases in the order of 6 M KOH >3 M KOH >1 M KOH. The enhancement in the specific capacity of the 3DG−SnO_2−TiO_2 nanocomposite in 6 M KOH can be attributed to the concentration of the ions in the electrolyte. The conductivity of the electrolyte can be increased by increasing its concentration in aqueous solution. Therefore, 6 M KOH provided higher conductivity and more enough OH^- concentration compared to 1 and 3 M solutions, which facilitates the charge transfer in both the bulk electrolyte and electrode.[32] This happens as the number of ions participating in the redox reactions increases. The 6 M KOH electrolyte possesses a high current value, resulting in a higher capacitance.[33]

To compare the electrochemical performance of the 3DG−SnO_2−TiO_2 ternary nanocomposite with the SnO_2−TiO_2 binary nanocomposite, working electrodes based on the SnO_2−TiO_2 binary nanocomposite and 3DG-SnO_2−TiO_2 ternary nanocomposite were made, and their electrochemical performances were investigated. CV curves at a lower scan rate (3 mV s^{-1}) for the binary and ternary composites are compared in Figure 7a. The CV curves at lower voltages indicate the redox process involving both the charge storage processes. The asymmetry in the CV curve shows that the charge storage process is battery-type.[34] The multiple redox peaks in the ternary composite can be attributed to the faradaic reaction involving the metal oxide and the solvated ions during the charge−discharge process. In general, the redox peaks occurred due to the insertion/de-insertion of the K^+ ions in/out of the composite oxides with concomitant oxidation/reduction of the Sn and Ti ions.[10] The 3DG−SnO_2−TiO_2 CV curves exhibit well-defined redox peaks compared with the SnO_2−TiO_2 CV curves.

The specific capacity of the electrode material from the CV curves was estimated using eq 1 and summarized in Table 1:

$$Q_S = \frac{\int i(E)\mathrm{d}E}{\mathrm{vm}} \quad (1)$$

https://doi.org/10.1021/acsomega.2c05343
ACS Omega 2022, 7, 43981−43991

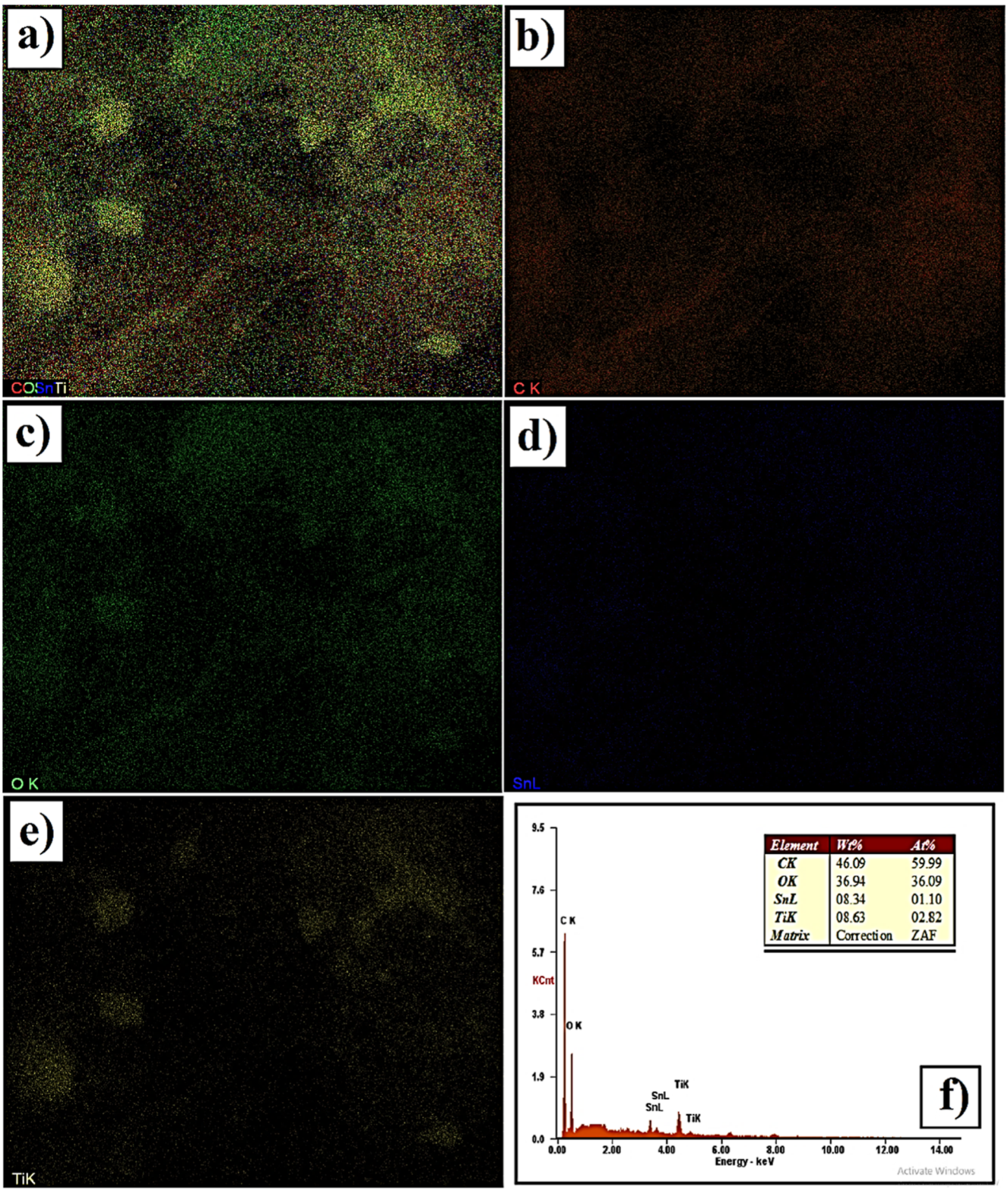

Figure 5. (a–e) Elemental mapping analysis and (f) EDX image of the 3DG–SnO_2–TiO_2 ternary nanocomposite.

where Q_S is the specific capacity (C g^{-1}) of the electrode material, $i(E)$ is the current, ν is the scan rate (V s^{-1}), and m is the mass loading (g) of the active material coated on the electrode.

Based on the calculated values, the ternary nanocomposite of 3DG–SnO_2–TiO_2 has a higher specific capacity at different scan rates when compared to the binary nanocomposite of SnO_2–TiO_2. Due to the inability of the solvated ions to access the active sites at higher current rates, the specific capacity of both electrode materials decreased as the scan rate increased (Table 1). At a lower scan rate, the solvated ion can access both the outer and inner pores of the electrode materials, increasing the intercalation reaction. The higher specific capacitance of the 3DG–SnO_2–TiO_2 ternary nanocomposite

https://doi.org/10.1021/acsomega.2c05343
ACS Omega 2022, 7, 43981–43991

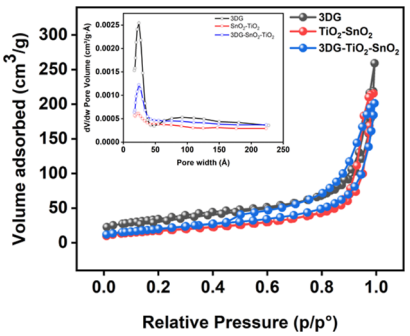

Figure 6. BET analysis of 3DG, SnO_2-TiO_2, and 3DG−SnO_2-TiO_2.

electrode materials compared with the SnO_2-TiO_2 binary nanocomposite can be attributed to both the faradaic contribution due to the charge-transfer process with the surface atoms (SnO_2 and TiO_2) and the nonfaradaic contribution from the double-layer effect (arising from 3DG).[35] The faradaic reactions of the SnO_2-TiO_2 nanocomposite are related to the following reversible process:

$$TiO_2 + C^+ + e^- \leftrightarrow TiOOC \quad (2)$$

$$SnO_2 + C^+ + e^- \leftrightarrow SnOOC \quad (3)$$

where C^+ are the protons and alkali metal cations (K^+) in the electrolyte (KOH). Based on the above reactions, it is suggested that both the protons and alkali metal cations are involved in the redox process.[36] Furthermore, the presence of 3DG in the nanocomposite provides a support matrix for the growth of the electroactive species at the nanoscale, which results in a larger specific surface area and thus enhances the electrochemical performance.[37]

The origin of capacitance in the material is determined from the CV curves by analyzing the dependence between the anodic peak current (i) and scan rate (ν). A straight line was obtained from $(\nu)^{1/2}$ and the anodic peak current (i), proving the domination of diffusion or intercalation reaction for both the binary and ternary composite electrodes (Figure S2) in 6 M KOH. The diffusion coefficient of all the electrodes will be obtained from the slope of the i versus $\nu^{1/2}$ graph, as detailed in our earlier research.[38] It was observed that the slope determined from the i versus $\nu^{1/2}$ graph for the 3DG−SnO_2-TiO_2 electrodes was an order higher (0.07) than the slope of the SnO_2-TiO_2 electrode (0.008). This proved that the introduction of 3DG to the secondary composite improved the solvated ion diffusion and hence the charge storage process.

Table 1. Specific Capacity of the SnO_2-TiO_2 Binary Nanocomposite and 3DG−SnO_2-TiO_2 Ternary Nanocomposite at the Range of Scan Rate of 3−50 mV s^{-1} in 6 M KOH

	specific capacity (C g^{-1})	
scan rate (mV s^{-1})	SnO_2-TiO_2	3DG−SnO_2-TiO_2
3	46.16	322.45
5	39.60	285.63
10	30.47	235.28
20	22.63	177.68
30	19.03	150.96
40	16.78	127.41
50	14.69	110.43

GCD curves were used to investigate the specific capacity of the prepared electrode materials (Figure 7b). The charge−discharge curves of the ternary composite electrode at 1 A g^{-1} were more symmetric compared to the binary composite electrode, demonstrating the superior charge storage of 3DG−SnO_2-TiO_2 electrodes. The electrode based on the SnO_2-TiO_2 binary nanocomposite shows a decrease in charging and discharging time with increasing current density, indicating that capacity decreases with increasing current density. The

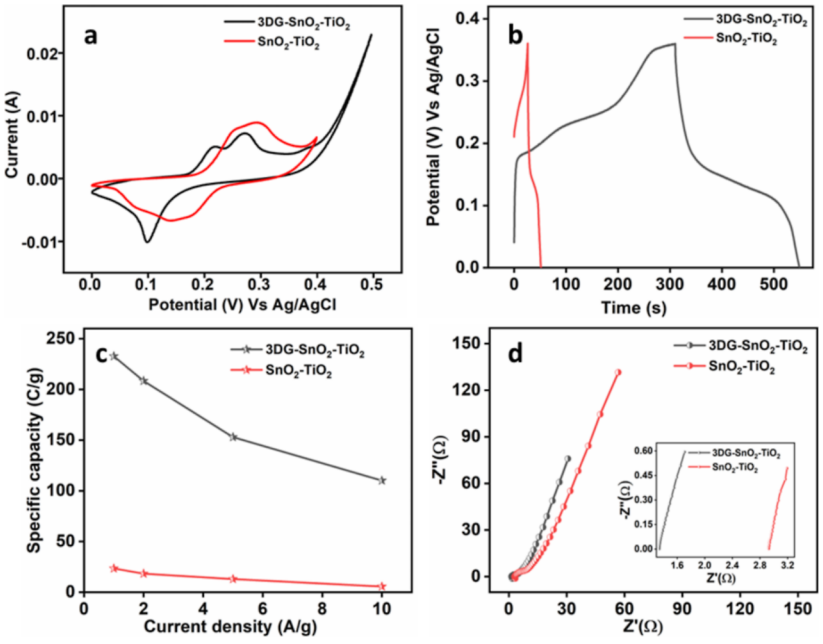

Figure 7. (a) Comparison of CV curves of the 3DG−SnO_2-TiO_2 ternary nanocomposite and SnO_2-TiO_2 binary nanocomposite at 3 mV s^{-1}. (b) Comparison of GCD curves of both the electrodes at 1 A g^{-1}. (c) Variation of capacitance of both the electrodes with different current densities. (d) Nyquist plots of both the electrodes, and the inset is the plot at higher frequencies.

https://doi.org/10.1021/acsomega.2c05343
ACS Omega 2022, 7, 43981−43991

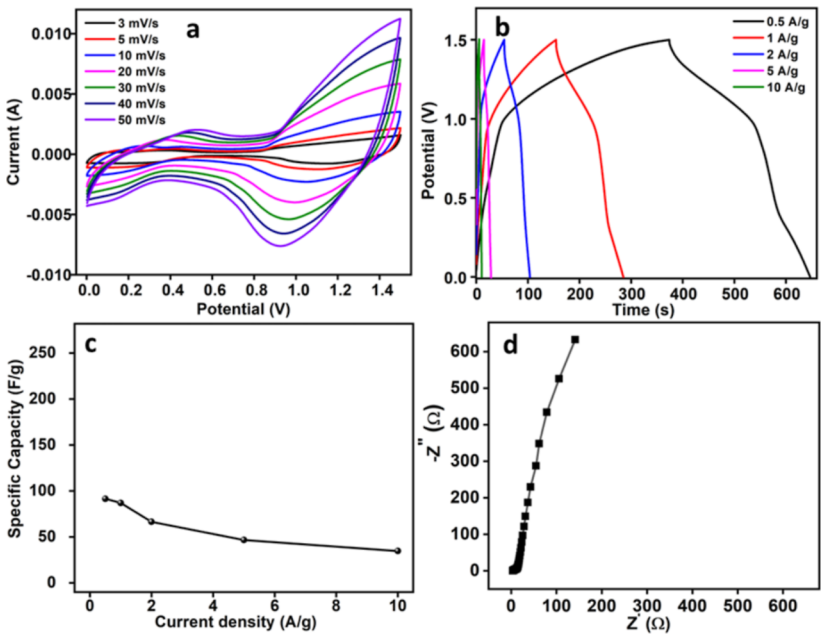

Figure 8. (a) CV curves of a 3DG−SnO_2−TiO_2//AC ASC device at different scan rates (3−50 mV s^{-1}); (b) GCD curves of a 3DG−SnO_2−TiO_2//AC device assessed at different current densities; (c) variation of specific capacitance of the ASC device at different current densities; (d) Nyquist plot of the 3DG−SnO_2−TiO_2//AC ASC device.

specific capacity of the electrode materials (Q_S) using 6 M KOH as an electrolyte is estimated using the following relation (equation 4):

$$Q\,s = \frac{I \times \Delta t}{m} \tag{4}$$

where I is defined as the discharge current (A), Δt is the time the electrode needs to be fully discharged, and m is the mass loading of the materials on the coated electrode.

A maximum specific capacity of 232.7 C g^{-1} is obtained for the 3DG−SnO_2−TiO_2 ternary nanocomposite at a current density of 1 A g^{-1}. At the same current density, the binary SnO_2−TiO_2 could achieve only a capacitance of ∼23.5 C g^{-1}. This demonstrated the importance of addition of 3DG to the binary composite material. In the 3DG−SnO_2−TiO_2 ternary nanocomposite, 3DG acts as a support matrix to develop electroactive species in the nanocomposite, which has a larger surface area and therefore improves the electrochemical performance.[39] Furthermore, the pore size of the ternary composite was more convenient for the solvated ion access of the KOH ions. The solvated ion size of K^+ ions (13 nm) was comparable with the pore size (17 nm) of the ternary nanocomposite and hence delivers a higher capacitance.[40] Also, the ionic conductivity of 6 M KOH is larger (626.6 mS cm^{-1}) compared to 3 M KOH and 1 M KOH.[41] Hence, the ternary composite electrode delivered a higher capacitance in 6 M KOH.

Similar to the variation of specific capacity with the scan rates, the specific capacity of both the electrodes decreased with the increase in the scan rate (Figure 7c). For the SnO_2−TiO_2 binary nanocomposite, the increase in current density results in a decrease in the charge and discharge times in the GCD curves of the 3DG−SnO_2−TiO_2 nanocomposite. The specific capacity of the SnO_2−TiO_2 nanocomposite decreased to 18.3, 12.95, and 5.6 C g^{-1} at the current density of 2, 5, and 10 A g^{-1}, as calculated using eq 2. The binary composite electrode could only retain 24% of its initial capacitance with 10 times increase in current density. Compared with the SnO_2−TiO_2 binary nanocomposite charge−discharge curves, the 3DG−SnO_2−TiO_2 ternary nanocomposite exhibited superior charge retention. At current densities of 2, 5, and 10 A g^{-1}, the specific capacities of the as-prepared 3DG−SnO_2−TiO_2 electrode are reduced to 208.4, 152.93, and 110.05 C g^{-1}, respectively. The 3DG−SnO_2−TiO_2 electrode could retain a specific capacity of ∼48% of its initial capacitance with an increase in current density from 1 to 10 A g^{-1}. This showed that the capacitance retention of SnO_2−TiO_2 almost doubled with the incorporation of 3DG. The decrease in capacitance for both the electrodes with the increase in current density could be attributed to the charge concentration at the electrode−electrolyte interface during the charge storage process.[42]

Electrochemical impedance spectroscopy (EIS) measures the characteristic resistances such as electrode resistance (R_S) and charge-transfer resistance (R_{CT}) during the charge-transfer process. R_S combines the electrolyte resistance, intrinsic resistance of the electroactive material, and contact resistance between the active material and the current collector to determine the high frequency of the EIS spectrum. The R_S value is calculated from the x-intercept of the high-frequency region of the Nyquist plot. The EIS plot of the SnO_2−TiO_2 binary nanocomposite is compared with the EIS plot of the 3DG−SnO_2−TiO_2 ternary nanocomposite in Figure 7d. The values of R_S determined from the high frequency of the EIS spectra for SnO_2−TiO_2 and 3DG−SnO_2−TiO_2 nanocomposites in 6 M KOH are 2.9 and 1.3 Ω, respectively. The ternary nanocomposite of the 3DG−SnO_2−TiO_2 electrode has a smaller semicircle in the high-frequency region than the binary nanocomposite of SnO_2−TiO_2, confirming that the electrode material based on the ternary nanocomposite has the lowest charge-transfer resistance (inset of Figure 7d). The lower electrode resistance of the ternary nanocomposite would have enhanced the electrode−electrolyte ion access and hence delivered a superior specific capacity compared to the binary

https://doi.org/10.1021/acsomega.2c05343
ACS Omega 2022, 7, 43981−43991

composite. Furthermore, the higher surface area of the ternary nanocomposite compared to the binary nanocomposite of SnO_2-TiO_2 would have increased the electrochemical performance of the 3DG−SnO_2-TiO_2 ternary nanocomposite. Intercalation of SnO_2-TiO_2 with 3DG provides more active sites for rapid redox processes, and the presence of 3DG in the composite can effectively prevent the degradation of the SnO_2-TiO_2 nanocomposite.[14]

4. CHARACTERIZATION OF ASYMMETRIC SUPERCAPACITORS

An asymmetric supercapacitor (ASC) is made up of two electrodes separated by an electrolyte ion separator, with capacitive materials such as activated carbon serving as the negative electrode and a ternary nanocomposite of 3DG−SnO_2-TiO_2 serving as the positive electrode. This combines the effects of a capacitor and a battery in a single device to gain the benefits of both systems, resulting in a higher energy density than that of a typical EDLC.[32] The 3DG−SnO_2-TiO_2 ternary nanocomposite and activated carbon (3DG−SnO_2-TiO_2//AC) were used as positive and negative electrodes, respectively. The fabricated device was then electrochemically analyzed at room temperature. Figure 8a shows the CV curves at various scan rates (3−100 mV s^{-1}). Furthermore, even at higher scan rates, the shape of the CV curves is well preserved, which demonstrates the excellent rate capability of the device. The ASC was built based on the mass loading calculation shown in eq 5

$$\frac{m_-}{m_+} = \frac{Q_{S+}(\mathrm{PC}) \times \Delta V}{Q_{S-}(\mathrm{EDLC}) \times \Delta V} \tag{5}$$

where m_- and Q_{S-} are the mass loading and specific capacity of the negative electrode; $m_+$and Q_{S+} are the mass loading and specific capacity of the positive electrode; and ΔV is the potential window. Figure S5 shows the electrochemical characterization of AC in 6 M KOH. The specific capacitance of AC was calculated to be 84 F g^{-1} at 1 A g^{-1}. Using eq 5, the AC and 3DG−SnO_2-TiO_2 mass loadings in ASC were determined to be approximately 1.38 and 2.85 mg, respectively. Cyclic voltammetry (CV), galvanic charge−discharge (GCD), and electrochemical impedance spectroscopy (EIS) were used to investigate the electrochemical performance of AC as a cathode (Supporting Information S5). The AC electrode CV curves show EDLC charge storage with no redox peaks (Figure S5a). The GCD curves (Figure S5b) and Nyquist plot (Figure S5c) illustrate a typical EDLC process, indicating that the electrode is an appropriate negative electrode for the ASC.

Figure 8b shows the GCD curves of the ASC at various current densities (0.5, 1.0, 2.0, 5.0, and 10.0 A g^{-1}) at a potential window of 1.5 V. The nonlinear GCD curves demonstrate the presence of faradaic reactions during charge−discharge. The electrochemical behavior of the fabricated ASC was highly reversible. The specific capacity of the ASC was calculated using eq 4, and the variation of specific capacitance of the ASC device at different current densities is indicated in Figure 8c. It can be observed from Figure 8c that the specific capacity of the ASC device is decreased with the increase in scan rate. At the current density of 0.5 A g^{-1}, the specific capacity is calculated to be 137.3 C g^{-1}.

To estimate the efficiency of the assembled device, the key parametric quantities are specific energy (E) and specific power (P), which have been calculated using eqs 6 and 7.

$$E(\mathrm{Wh/kg}) = \frac{\Delta V \times Q_S}{2 \times 3.6} \tag{6}$$

$$P(\mathrm{W/kg}) = \frac{E \times 3600}{\Delta t} \tag{7}$$

where ΔV (V) represents the potential range, Q_s (C g^{-1}) is the specific capacity, and Δt is the time required to fully discharge (s). A maximum energy density (E_D) of 28.6 Wh kg^{-1} is obtained at a power density (P_D) of 367.7 W kg^{-1} at 0.5 A g^{-1}, which is comparable with the reported carbon-based nanocomposites such as PANI−SnO_2-TiO_2//AC with energy density of 27 Wh kg^{-1},[8] MnO_2/CNT//AC with energy density of 23.2 Wh kg^{-1}.,[43] CoS/graphene//AC with energy density of 29 Wh kg^{-1},[44] and Al_2O_3-doped Co_3O_4/graphene//AC with energy density of 40.1 Wh kg^{-1}.[45]Figure 8d shows the Nyquist plot of ASC based on the 3DG−SnO_2-TiO_2 ternary nanocomposite in the frequency range from 0.01 to 100 kHz at an AC voltage of 10 mV. The EIS plot of the 3DG−SnO_2-TiO_2 ternary nanocomposite shows a semicircle in the high-frequency region and a straight line in the low-frequency region, as expected for an assembled ASC. The R_S value calculated from the high frequency EIS for the 3DG−SnO_2-TiO_2 ternary nanocomposite is 0.99. The semicircle diameter measurement indicates a low resistance of the cell, which implies a short charge-transfer path. The high slope of the line in the Nyquist plot in the low-frequency region shows a low interfacial diffusion resistance, implying fast ion diffusion and mass transport at the electrode/electrolyte interface.[46]

The cyclic stability of an ASC based on the 3DG−SnO_2-TiO_2 ternary nanocomposite at a current density of 5 A g^{-1} is shown in Figure 9. The ASC based on the prepared ternary

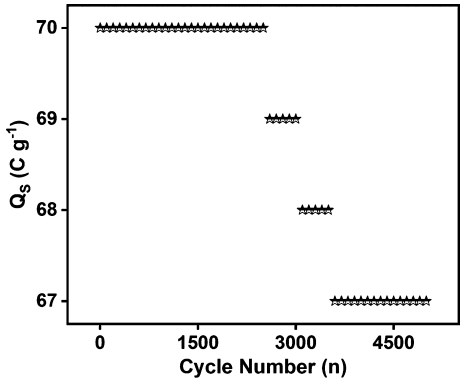

Figure 9. (a) Cycling stability of a 3DG−SnO_2-TiO_2//AC device at a current density of 5 A g^{-1} after 5000 cycles.

nanocomposite could retain ∼97% of its initial capacitance after 5000 cycles, which is a good indication of its high cyclic stability. Based on the results, the cyclic stability and surface area of the SnO_2-TiO_2 nanocomposite eventually improved by the incorporation of 3DG with the SnO_2-TiO_2 nanocomposite, which helps to make it a suitable material for energy storage devices.

Furthermore, the superiority of the present work over the other SnO_2-TiO_2 composites for supercapacitors could be observed from Table 2. Table 2 compares the specific

https://doi.org/10.1021/acsomega.2c05343
ACS Omega 2022, 7, 43981−43991

Table 2. Comparison of Specific Capacity and Cyclic Stability of SnO_2−TiO_2-Based Supercapacitors

materials	specific capacitance (F/g)	$Q_s$retention/cycle number	electrolyte	current density	ref
		three-electrode configuration			
3DG−PANI	346	70%/600	1 M H_2SO_4	4 A/g	47
3D−RGNi	1328	87%/2000	2 M KOH	1 A/g	15
SnO_2−TiO_2 nanoflowers	500		6 M KOH	1 A/g	10
SnO_2−TiO_2 nanofibers	350		6 M KOH	1 A/g	
3DG−SnO_2−TiO_2	284.5		1 M KOH	1 A/g	this work
	350.95		3 M KOH		
	665.70		6 M KOH		
		two-electrode configuration			
hydrogenation of TiO_2@GO	51.10	80%/10000	1 M Na_2SO_4	1 A/g	48
PANI−SnO_2−TiO_2	540	85%/6000	1 M H_2SO_4	0.35 A/g	8
3DG−TiO_2	64.90	90%/500	3 M KOH	0.2 A/g	16
3DG−SnO_2−TiO_2	91.53	97%/5000	6 M KOH	0.5 A/g	this work

capacitance and cyclic stability of the 3DG−SnO_2−TiO_2 ternary nanocomposite and the previously reported composite materials in two- and three-electrode configurations. For a better understanding, the specific capacity of the 3DG−SnO_2−TiO_2 electrode obtained in C g^{-1} was converted to specific capacitance in F g^{-1} using eq 8:

$$C_S = {Q_S}/{\Delta V} \quad (8)$$

Table 2 signifies that there were no earlier reports of an ASC based on the 3DG−SnO_2−TiO_2 composite/ASC. As both SnO_2 and TiO_2 materials are environmental friendly, easily available, and cheaper, the combination of both the materials into a 3DG matrix is significant. Furthermore, the fabricated ASC device shows appreciable energy and power density and a superior cycling stability. From Table 2, it can be observed that the ternary nanocomposite of 3DG−SnO_2−TiO_2 exhibited better rate capability compared to other nanocomposites. The improvement in the rate capability of the 3DG−SnO_2−TiO_2 ternary nanocomposite is because of the presence of 3DG that provides more active sites for the rapid electron transfer rate.

CONCLUSIONS

The 3DG−SnO_2−TiO_2 ternary nanocomposite prepared by the hydrothermal method indicated the highest specific capacity (232.7 C g^{-1}) in 6 M KOH compared to the SnO_2−TiO_2 binary nanocomposite (23.45 C g^{-1}) because of the successful incorporation of 3DG into the SnO_2−TiO_2 nanocomposite. The addition of the SnO_2−TiO_2 nanocomposite to the 3DG matrix enhanced the surface area and increased the specific capacity almost 10 times in comparison with the binary nanocomposite of SnO_2−TiO_2. Moreover, the presence of 3DG can effectively prevent the degradation of the SnO_2−TiO_2 nanocomposite and provide more active sites for a rapid redox process. An ASC was also made for the first time with the 3DG−SnO_2−TiO_2 composite, and the assembled device had a specific energy of 28.6 Wh kg^{-1} and a specific power of 367.7 Wkg^{-1} at a current density of 0.5 A g^{-1}. As a result, the ASC could retain 97% of its initial capacitance after 5000 cycles, demonstrating superior cycling stability. The electrochemical performance of the 3DG−SnO_2−TiO_2 ternary nanocomposite proves to be an appropriate candidate for electrodes in energy storage systems.

ASSOCIATED CONTENT

Supporting Information

The Supporting Information is available free of charge at https://pubs.acs.org/doi/10.1021/acsomega.2c05343.

CV curves of 3DG−SnO_2−TiO_2 composites in different molar KOH solutions; charge−discharge curves of 3DG−SnO_2−TiO_2 composites in different molar KOH solutions; diffusion-controlled charge storage process of the ternary and binary composites in 6 M KOH; Nyquist plots of 3DG−SnO_2−TiO_2 composites in different molar KOH solutions; electrochemical characterization of commercial AC in 6 M KOH; and determination of proper working potential for the ASC device (PDF)

AUTHOR INFORMATION

Corresponding Authors

Golnoush Zamiri − *Department of Mechanical Engineering, Faculty of Engineering, University of Malaya, 50603 Kuala Lumpur, Malaysia; Centre of Advanced Materials, Faculty of Engineering, University of Malaya, 50603 Kuala Lumpur, Malaysia;* orcid.org/0000-0003-4223-5062; Email: golnoush.Zamiri@um.edu.my

A.S. Md. Abdul Haseeb − *Department of Mechanical Engineering, Faculty of Engineering, University of Malaya, 50603 Kuala Lumpur, Malaysia; Centre of Advanced Materials, Faculty of Engineering, University of Malaya, 50603 Kuala Lumpur, Malaysia*; Email: haseeb@um.edu.my

Syam G. Krishnan − *Sustainable Energy Materials Lab, School of Chemistry and Physics, Faculty of Science, Queensland University of Technology, 4000 Brisbane, Queensland, Australia;* orcid.org/0000-0002-8549-4323; Email: syam.gopalakrishnan@qut.edu.au

Authors

Priyanka Jagadish − *Graphene & Advanced 2D Materials Research Group (GAMRG), School of Science and Technology, Sunway University, 47500 Subang Jaya, Selangor, Malaysia*

Mohammad Khalid − *Graphene & Advanced 2D Materials Research Group (GAMRG), School of Science and Technology, Sunway University, 47500 Subang Jaya, Selangor, Malaysia*

Ing Kong − *School of Engineering and Mathematical Sciences, La Trobe University, 3552 Bendigo, Victoria, Australia*

https://doi.org/10.1021/acsomega.2c05343
ACS Omega 2022, 7, 43981−43991

Complete contact information is available at:
https://pubs.acs.org/10.1021/acsomega.2c05343

Notes

The authors declare no competing financial interest.

■ ACKNOWLEDGMENTS

The authors acknowledge the financial support provided by the University of Malaya grant through the Postdoctoral Research Fellowship (G.Z.) and Impact-Oriented Interdisciplinary Research Programme (IIRG) (no.: IIRG018C-2019).

■ REFERENCES

(1) Iqbal, M. Z.; Faisal, M. M.; Ali, S. R.; Afzal, A. M. Hydrothermally synthesized zinc phosphate-rGO composites for supercapattery devices. *J. Electroanal. Chem.* **2020**, *871*, 114299.

(2) (a) Wang, G.; Zhang, L.; Zhang, J.; Yao, S. A review of electrode materials for electrochemical supercapacitors. *Chem. Soc. Rev.* **2012**, *41*, 797−828. (b) Zhu, Y. Nanomaterial-enabled stretchable conductors: strategies, materials and devices. *Adv. Mater.* **2015**, *27*, 1480−1511.

(3) Krishnan, S. G.; Archana, P. S.; Vidyadharan, B.; Misnon, I. I.; Vijayan, B. L.; Nair, V. M.; Gupta, A.; Jose, R. Modification of capacitive charge storage of TiO_2 with nickel doping. *J. Alloys Compd.* **2016**, *684*, 328−334.

(4) Dubal, D. P.; Ayyad, O.; Ruiz, V.; Gómez-Romero, P. Hybrid energy storage: the merging of battery and supercapacitor chemistries. *Chem. Soc. Rev.* **2015**, *44*, 1777−1790.

(5) (a) Stevenson, A. J.; Gromadskyi, D. G.; Hu, D.; Chae, J.; Guan, L.; Yu, L.; Chen, G. Z. Supercapatteries with hybrids of redox active polymers and nanostructured carbons. *Nanocarbons for Advanced Energy Storage* **2015**, *1*, 179−210. (b) Shao, H.; Padmanathan, N.; McNulty, D.; O'Dwyer, C.; Razeeb, K. M. Supercapattery based on binder-free Co3 (PO4) 2· 8H2O multilayer nano/microflakes on nickel foam. *ACS applied materials & interfaces* **2016**, *8*, 28592−28598.

(6) Krishnan, S. G.; Harilal, M.; Arshid, N.; Jagadish, P.; Khalid, M.; Li, L. P. Rapid microwave-assisted synthesis of $MnCo_2O_4$ nanoflakes as a cathode for battery-supercapacitor hybrid. *J. Energy Storage* **2021**, *44*, 103566.

(7) Krishnan, S. G.; Arulraj, A.; Khalid, M.; Reddy, M. V.; Jose, R. Energy storage in metal cobaltite electrodes: Opportunities & challenges in magnesium cobalt oxide. *Renewable and Sustainable Energy Reviews* **2021**, *141*, 110798.

(8) Bolagam, R.; Boddula, R.; Srinivasan, P. Hybrid material of PANi with TiO2-SnO2: pseudocapacitor electrode for higher performance supercapacitors. *ChemistrySelect* **2017**, *2*, 65−73.

(9) Fan, S.; Zhang, J.; Teng, X.; Wang, X.; Li, H.; Li, Q.; Xu, J.; Cao, D.; Li, S.; Hu, H. Self-supported amorphous SnO2/TiO2 nanocomposite films with improved electrochemical performance for lithium-ion batteries. *J. Electrochem. Soc.* **2019**, *166*, A3072.

(10) Pal, B.; Bakr, Z. H.; Krishnan, S. G.; Yusoff, M. M.; Jose, R. J. Large scale synthesis of 3D nanoflowers of SnO2/TiO2 composite via electrospinning with synergistic properties. *Mater. Lett.* **2018**, *225*, 117−121.

(11) Iqbal, J.; Numan, A.; Ansari, M. O.; Jagadish, P. R.; Jafer, R.; Bashir, S.; Mohamad, S.; Ramesh, K.; Ramesh, S. Facile synthesis of ternary nanocomposite of polypyrrole incorporated with cobalt oxide and silver nanoparticles for high performance supercapattery. *Electrochim. Acta* **2020**, *348*, 136313.

(12) Bose, S.; Kuila, T.; Mishra, A. K.; Rajasekar, R.; Kim, N. H.; Lee, J. H. Carbon-based nanostructured materials and their composites as supercapacitor electrodes. *RSC Adv.*, **2012**, *22*, 767−784.

(13) (a) Wang, Y.; Guo, C. X.; Liu, J.; Chen, T.; Yang, H.; Li, C. M. CeO 2 nanoparticles/graphene nanocomposite-based high performance supercapacitor. *Dalton Trans.* **2011**, *40*, 6388−91. (b) Ramadoss, A.; Yoon, K.-Y.; Kwak, M.-J.; Kim, S.-I.; Ryu, S.-T.; Jang, J.-H. Fully flexible, lightweight, high performance all-solid-state supercapacitor based on 3-Dimensional-graphene/graphite-paper. *J. Power Sources* **2017**, *337*, 159−165.

(14) Iqbal, J.; Numan, A.; Jafer, R.; Bashir, S.; Jilani, A.; Mohammad, S.; Khalid, M.; Ramesh, K.; Ramesh, S. Compounds. Ternary nanocomposite of cobalt oxide nanograins and silver nanoparticles grown on reduced graphene oxide conducting platform for high-performance supercapattery electrode material. *J. Alloys and Compounds* **2020**, *821*, 153452.

(15) Trung, N. B.; Tam, T.; Dang, D. K.; Babu, K. F.; Kim, E. J.; Kim, J.; Choi, W. M. Facile synthesis of three-dimensional graphene/nickel oxide nanoparticles composites for high performance supercapacitor electrodes. *Chem. Eng. J.* **2015**, *264*, 603−609.

(16) Li, S.; Jiang, H.; Yang, K.; Zhang, Z.; Li, S.; Luo, N.; Liu, Q.; Wei, R. Compounds. Three-dimensional hierarchical graphene/TiO2 composite as high-performance electrode for supercapacitor. *J. Alloys Compd.* **2018**, *746*, 670−676.

(17) Kim, Y.-R.; Bong, S.; Kang, Y.-J.; Yang, Y.; Mahajan, R. K.; Kim, J. S.; Kim, H. Electrochemical detection of dopamine in the presence of ascorbic acid using graphene modified electrodes. *Biosens. Bioelectron.* **2010**, *25*, 2366−2369.

(18) Babadi, A. A.; Wan-Mohtar, W. A. A. Q. I.; Chang, J.-S.; Ilham, Z.; Jamaludin, A. A.; Zamiri, G.; Akbarzadeh, O.; Basirun, W. J. High-performance enzymatic biofuel cell based on three-dimensional graphene. *Int. J. Hydrogen Energy* **2019**, *44*, 30367−30374.

(19) Zamiri, G.; Haseeb, A.; Krishnan, S. G.; Numan, A.; Jagadish, P.; Khalid, M. Ternary nanocomposite cathodes based on 3D graphene-Ag nanoparticle-polyaniline for hybrid electrochemical energy device. *Synthetic Metals* **2021**, *282*, 116932.

(20) Messaadi, C.; Ghrib, T.; Jalali, J.; Ghrib, M.; Alyami, A. A.; Gaidi, M.; Silvan, M. M.; Ezzaouia, H. J. C. N. Synthesis and Characterization of SnO2-TiO2 Nanocomposites. *Photocatalysts* **2019**, *15*, 398−406.

(21) Bondavalli, P.*Graphene and related nanomaterials: properties and applications*; Elsevier, 2017.

(22) Syama, S.; Mohanan, P. V. Comprehensive application of graphene: emphasis on biomedical concerns. *Nano-Micro Lett.* **2019**, *11*, 1−31.

(23) Kunthadee, P.; Phaphan, M.*Iron (III)-selective optical sensor based on plasticized membrane incorporating ethyl protocatechuate compared with naked-eye screening method*, 2020.

(24) Meng, Y.; Wang, K.; Zhang, Y.; Wei, Z. Hierarchical porous graphene/polyaniline composite film with superior rate performance for flexible supercapacitors. *Adv. Mater.*, **2013**, *25*, 6985−6990.

(25) Mohammad, A.; Khan, M. E.; Cho, M. H.; Yoon, T. Fabrication of binary SnO2/TiO2 nanocomposites under a sonication-assisted approach: Tuning of band-gap and water depollution applications under visible light irradiation. *Ceram. Int.* **2021**, *47*, 15073−15081.

(26) Jia, Y.; Hu, D.; Wang, X.; Zhang, H.; Du, P. Carbon layer coated nickel phosphide nanoparticles embedded in three-dimensional graphene network for high-performance supercapacitor. *J. Energy Storage* **2022**, *50*, 104713.

(27) Fang, S.; Huang, D.; Lv, R.; Bai, Y.; Huang, Z.-H.; Gu, J.; Kang, F. Three-dimensional reduced graphene oxide powder for efficient microwave absorption in the S-band (2−4 GHz). *RSC Advances.* **2017**, *7*, 25773−25779.

(28) Challagulla, S.; Tarafder, K.; Ganesan, R.; Roy, S. Structure sensitive photocatalytic reduction of nitroarenes over TiO 2. *Sci. Rep.* **2017**, *7*, 1−11.

(29) Zhao, Q.; Ju, D.; Deng, X.; Huang, J.; Cao, B.; Xu, X. J. S. r. Morphology-modulation of SnO2 hierarchical architectures by Zn doping for glycol gas sensing and photocatalytic applications. *Sci. Rep.* **2015**, *5*, 1−9.

(30) (a) Zazouli, M. A.; Yousefi, M.; Ghanbari, F.; Babanezhad, E. Engineering. Performance of photocatalytic ozonation process for pentachlorophenol (PCP) removal in aqueous solution using graphene-TiO2 nanocomposite (UV/G-TiO2/O3). *J Environ Health Sci Eng.* **2020**, *18*, 108−109. (b) Stepić, K.; Ljupković, R.; Ickovski, J.;

https://doi.org/10.1021/acsomega.2c05343
ACS Omega 2022, 7, 43981−43991

Zarubica, A. A short review of titania-graphene oxide based composites as a photocatalysts. *Adv. Technol.* **2021**, *10*, 351−760.
(31) Kunwar, R.; Krishnan, S. G.; Misnon, I. I.; Zabihi, F.; Yang, S.; Yang, C.-C.; Jose, R. Transformation of Supercapacitive Charge Storage Behaviour in a Multi elemental Spinel $CuMn_2O_4$ Nanofibers with Alkaline and Neutral Electrolytes. *Adv Fiber Materials* **2021**, *3*, 265−274.
(32) Zhao, Y.; Hao, M.; Wang, Y.; Sha, Y.; Su, L. Effect of electrolyte concentration on the capacitive properties of NiO electrode for supercapacitors. *J. Solid State Electrochem.* **2016**, *20*, 81−85.
(33) Nithya, V.; Kalai Selvan, R. K.; Kalpana, D.; Vasylechko, L.; Sanjeeviraja, C. Synthesis of Bi2WO6 nanoparticles and its electrochemical properties in different electrolytes for pseudocapacitor electrodes. *Electrochimica Acta.* **2013**, *109*, 720−731.
(34) Chodankar, N. R.; Pham, H. D.; Nanjundan, A. K.; Fernando, J. F. S.; Jayaramulu, K.; Golberg, D.; Han, Y.-K.; Dubal, D. P. True Meaning of Pseudocapacitors and Their Performance Metrics: Asymmetric versus Hybrid Supercapacitors. *Small* **2020**, *16*, 2002806.
(35) Ramadoss, A.; Kim, S. J. Improved activity of a graphene−TiO2 hybrid electrode in an electrochemical supercapacitor. *Carbon.* **2013**, *63*, 434−445.
(36) Wei, Z.; Liu, M.; Li, H.; Sun, S.; Yang, L. J. SnO2 quantum dots decorated reduced graphene oxide nanosheets composites for electrochemical supercapacitor applications. *Int. J. Electrochem. Sci.* **2020**, *15*, 6257−6268.
(37) Raccichini, R.; Varzi, A.; Passerini, S.; Scrosati, B. The role of graphene for electrochemical energy storage. *Nat. Mat.* **2015**, *14*, 271−279.
(38) Krishnan, S. G.; Reddy, M. V.; Harilal, M.; Vidyadharan, B.; Misnon, I. I.; Rahim, M. H. A.; Ismail, J.; Jose, R. Characterization of $MgCo_2O_4$ as an electrode for high performance supercapacitors. *Electrochim. Acta* **2015**, *161*, 312−321.
(39) Nandi, D.; Mohan, V. B.; Bhowmick, A. K.; Bhattacharyya, D. Metal/metal oxide decorated graphene synthesis and application as supercapacitor: a review. *J. Mater. Sci.* **2020**, *55*, 6375−6400.
(40) Misnon, I. I.; Aziz, R. A.; Zain, N. K. M.; Vidhyadharan, B.; Krishnan, S. G.; Jose, R. High performance MnO_2 nanoflower electrode and the relationship between solvated ion size and specific capacitance in highly conductive electrolytes. *Mater. Res. Bull.* **2014**, *57*, 221−230.
(41) Vidhyadharan, B.; Misnon, I. I.; Aziz, R. A.; Padmasree, K. P.; Yusoff, M. M.; Jose, R. Superior supercapacitive performance in electrospun copper oxide nanowire electrodes. *J. Mater. Chem. A* **2014**, *2*, 6578−6588.
(42) Vivek, E.; Arulraj, A.; Krishnan, S. G.; Khalid, M.; I, V. P. Novel Nanostructured $Nd(OH)_3$/g-C_3N_4 Nanocomposites (Nanorolls Anchored on Nanosheets) as Reliable Electrode Material for Supercapacitors. *Energy Fuels* **2021**, *35*, 15205−15212.
(43) Xia, H.; Huo, C. Materials Electrochemical properties of MnO2/CNT nanocomposite in neutral aqueous electrolyte as cathode material for asymmetric supercapacitors. *Emergent Materials* **2011**, *2*, 283−291.
(44) Shi, J.; Li, X.; He, G.; Zhang, L.; Li, M. J. Electrodeposition of high-capacitance 3D CoS/graphene nanosheets on nickel foam for high-performance aqueous asymmetric supercapacitors. *J. Mater. Chem. A* **2015**, *3*, 20619−20626.
(45) Zhang, G.-F.; Qin, P.; Song, J.-M. Facile fabrication of Al2O3-doped Co3O4/graphene nanocomposites for high performance asymmetric supercapacitors. *Appl. Surf. Sci.* **2019**, *493*, 55−62.
(46) Mei, B.-A.; Munteshari, O.; Lau, J.; Dunn, B.; Pilon, L. J. Physical interpretations of Nyquist plots for EDLC electrodes and devices. *J. Phys. Chem. C* **2018**, *122*, 194−206.
(47) Dong, X.; Wang, J.; Wang, J.; Chan-Park, M. B.; Li, X.; Wang, L.; Huang, W.; Chen, P. Physics. Supercapacitor electrode based on three-dimensional graphene−polyaniline hybrid. *Mater. Chem. Phys.* **2012**, *134*, 576−580.
(48) Pham, V. H.; Nguyen-Phan, T.-D.; Tong, X.; Rajagopalan, B.; Chung, J. S.; Dickerson, J. H. J. C. Hydrogenated TiO2@ reduced graphene oxide sandwich-like nanosheets for high voltage supercapacitor applications. *Carbon* **2018**, *126*, 135−144.

https://doi.org/10.1021/acsomega.2c05343
ACS Omega 2022, 7, 43981−43991